Classical and quantum aspects of spin interaction in 3*d* chains on a Cu₃N-Cu(110) molecular network

D. I. Bazhanov,[1,2,3] O. V. Stepanyuk,[1,3] O. V. Farberovich,[4,5] and V. S. Stepanyuk[1]

[1]*Max-Planck-Institut für Mikrostrukturphysik, Weinberg 2, D-06120 Halle, Germany*
[2]*Faculty of Physics, Moscow State University, GSP-1, Lenin Hills, 119991 Moscow, Russia*
[3]*Institution of Russian Academy of Sciences, Dorodnicyn Computing Centre of RAS, Vavilov st. 40, 119333 Moscow, Russia*
[4]*School of Physics and Astronomy, Beverly and Raymond Sackler Faculty of Exact Sciences, Tel Aviv University, Tel Aviv 69978, Israel*
[5]*Research Center for Nanoscale Structure of Matter, Southern Federal University, Zorge 5, 344090 Rostov-on-Don, Russia*

We present a study of the magnetic states and exchange coupling in transition-metal Mn, Fe, and Co atomic chains deposited on a self-corrugated Cu₃N-Cu(110) molecular network by means of first-principles calculations based on the density functional theory. The various adsorption sites on a bumping area of a self-corrugated Cu₃N layer are investigated where the atomic chains are formed at the initial stage of nanowire growth. We demonstrate, by calculating the ground-state magnetic configurations, that the exchange coupling, magnetic order, and anisotropies in atomic chains depend sensitively on their chemical composition and adsorption sites on the Cu₃N network. We find that the exchange interactions in atomic chains could lead to ferromagnetic or antiferromagnetic coupling of atomic spins depending on the position of the chain on the surface. The classical spin dynamics is investigated by means of the kinetic Monte Carlo method based on transition-state theory. Moreover we evaluate the Heisenberg–Dirac–Van Vleck quantum spin Hamiltonian for calculations of the magnetic susceptibility, in order to demonstrate the existence of quantum entanglement in the antiferromagnetic atomic chains at low temperatures.

I. INTRODUCTION

During the past decades atomic-scale magnetic nanostructures adsorbed on various substrates have attracted an essential interest both for basic and applied research [1]. These nanostructures consisting of only few individual atoms or clusters exhibit intriguing magnetic properties related with a large net spin moment and magnetocrystalline anisotropy, spin excitations, and spin coupling via direct overlap, superexchange, or Ruderman-Kittel-Kasuya-Yosida (RKKY) interaction, leading the neighboring spins to ferromagnetic or antiferromagnetic alignments [2,3]. Due to that, there are a lot of discussions in the literature about technologically relevant applications of these magnetic nanostructures as novel magnetic storage bits in the development of atomic-scale data-storage devices with a feasible small size and high magnetic recording density. Recent achievements in surface science techniques, based on the scanning tunneling microscope (STM), allowed to probe and manipulate just single magnetic atoms placed on substrates and to measure the key physical quantities determining their spin coupling and magnetic anisotropy energies (MAEs) with atomic-scale precision [4]. In a pioneering work of Heinrich *et al.*, it was demonstrated beautifully that the spin excitation spectra of individual Mn atoms on a surface can be measured using the inelastic electron-tunneling spectroscopy (IETS) with STM [5]. Later on, STM was used to probe the interactions between spins within linear chains of up to ten Mn atoms assembled by atomic manipulation on a thin copper nitride insulating layer grown on a Cu(001) surface [to be referenced as CuN₂/Cu(001) in this paper] [6]. Performing IETS again, the authors demonstrated the significant changes in spin-flip spectra for Mn atoms placed on the different binding sites upon which the chains were built on the surface. The low-temperature STM measurements showed that Mn

atoms are antiferromagnetically coupled and the strength of this coupling depends strongly on deposition sites. Moreover the collective spin configurations were well estimated directly for those chains using the model spin Hamiltonian. Such phenomenological approach was later applied successfully by Hirjibehedin *et al.* to explore the spin orientation and the strength of magnetic anisotropies for individual Fe and Mn atoms placed onto a CuN₂/Cu(001) surface [7]. It was shown that magnetic atoms embedded strongly into a polar covalent surface network in the copper nitride and possessed large enough magnetic anisotropy energies per single atom. These experimental and theoretical findings revealed the potential ability to produce at low temperatures the magnetic systems in which a spin coupling and a large magnetic anisotropy can be engineered at the atomic scale. Later on, STM studies by Otte *et al.* were carried out in order to explore simultaneously the atomic spin value, magnetic anisotropy, and the Kondo properties for individual Co and Ti atoms adsorbed on a CuN₂/Cu(001) surface [8,9]. The obtained conductance spectra of these atoms showed clearly the decisive role of the magnetic anisotropy and spin coupling in forming the Kondo screening. Further exciting extensions in research were presented in the recent paper of Loth *et al.* [10]. The authors observed magnetic bistability (transition between two Néel states) for antiferromagnetic chains, assembled from just six Fe atoms on a copper nitride surface, in which the orientation of an atomic spin was alternating between neighboring atoms. These two magnetic states were found to be stable for hours at low temperature. It was possible to switch between them electrically with nanosecond speed. Recently it was also demonstrated that one can controllably enhance or reduce magnetic anisotropy of individual Fe atoms placed onto a CuN₂/Cu(001) surface by adjusting the relative atomic

position of a second nearby Fe atom using atom manipulation in a low-temperature STM [11].

The mentioned experimental studies of magnetic nanostructures on a CuN_2/Cu(001) surface were followed by a few theoretical ones of this system based on density functional theory (DFT). Most of them were focused so far on the verification of experimental findings and studying the additional properties of interest for such system. For example, Shick *et al.* studied the magnetic anisotropies of individual Mn, Fe, and Co atoms using the first-principles calculations in local spin density (LSDA) and LDA+U approximations implemented in the relativistic version of the full-potential–linearized augmented plane-wave (FP-LAPW) method [12,13]. It was shown that the calculated MAE and direction of easy magnetization are in a reasonable agreement with experiment. The first-principles study of the structural, electronic, and magnetic properties of Mn isolated atoms and dimers on a copper nitride surface have been performed by Scopel *et al.* within the generalized gradient approximation (GGA) and pseudopotentials approach [14]. The obtained results showed that these adsorbates caused significant local structural changes on surface and spin coupling between Mn atoms depending strongly on whether they were placed on top of N or Cu atoms. Besides, Rudenko *et al.* have found a weak ferromagnetism for Mn chains (up to four atoms) sitting on Cu sites of a CuN_2/Cu(001) surface using the first-principles LSDA and LDA+U calculations [15]. Lin *et al.* recently applied the GGA+U approach in order to compare the magnetic behavior of Mn and Co adatoms on a CuN_2/Cu(001) surface [16]. The performed calculations of the electronic and spin structures showed clearly that the Mn and Co atoms preserve on such surface their spins $S = 5/2$ and $S = 3/2$, respectively, in agreement with the indirect STM measurements. Using that, it was explained why Co exhibits a Kondo effect, while Mn does not. Later on, Nicklas *et al.* reported the first-principles study of the magnetic anisotropies and spin coupling for Fe chains (up to three atoms) placed on top of the Cu atoms of a CuN_2/Cu(001) surface using the projector augmented-wave (PAW) method and pseudopotentials approach [17]. The calculated MAE for single Fe atom was found to be in excellent agreement with experiments. The results for spin coupling strength for Fe dimer and trimer established antiferromagnetic states occurred due to a superexchange interaction mediated by nitrogen atoms of the decoupling copper nitride layer. However, a ferromagnetic coupling was found on this surface for the Ti dimer due to a superexchange over N atoms by Pushpa *et al.* [18]. A recent systematic study of spin coupling, based on the full-potential–linearized augmented plane-wave (FP-LAPW) method, was reported for monatomic 3d (Cr, Mn, Fe, and Co) chains placed on a CuN_2/Cu(001) surface [19]. It was shown that different types of bonding on the decoupling copper nitride layer determine the kind of magnetic interaction between 3d atomic spins within the chain, while the d-band filling determines the final magnetic ground state. These results demonstrated a richness in the magnetic interactions on the copper nitride surface which can be very promising in the future for spin engineering at the atomic scale.

In the present paper we perform a first-principles study of the exchange interactions, magnetic anisotropies, and spin

dynamics of monatomic Mn, Fe, and Co chains placed on a self-corrugated Cu_3N/Cu(110) surface (to be referenced as Cu_3N in this paper). It was shown in our previous combined experimental and theoretical study that this substrate is formed by a reconstructed covalently bonded molecular Cu_3N network growing on a single-crystalline Cu(110) surface, which exhibits an insulating behavior with a band gap exceeding 3 eV, that is similar to the copper nitride CuN_2 on a Cu(001) surface [20]. Moreover such substrate can serve as a good template which can be employed so far to self-assemble metallic chains with universal growth behavior. We show that Cu_3N/Cu(110) offers another interesting covalently bonded copper nitride surface to tailor magnetic interactions and anisotropies among transition-metal atoms. We demonstrate that both ferromagnetic and antiferromagnetic 3d chains with large magnetic anisotropies can exist on this surface. For the antiferromagnetic chains the quantum entanglement is predicted.

II. DETAILS OF DFT CALCULATIONS AND DESCRIPTION OF SYSTEM

We perform the first-principles calculations based on density functional theory as it is implemented in the Vienna *ab initio* simulation package (VASP) [21]. The VASP code was used to solve self-consistently Kohn-Sham equations with periodic boundary conditions and a plane-wave basis set. For total energy and force calculations, we employed an all-electron projector augmented wave (PAW) method [22]. Spin-orbit interactions were included in our calculations. The maximal kinetic energy cutoff for plane waves of 400 eV was used to describe the electronic states in the system. The generalized gradient approximation (GGA) for the exchange-correlation functional has been applied using the Perdew-Wang '91 treatment [23]. The Monkhorst-Pack scheme [24] was employed for k-point sampling of the Brillouin zone (BZ), while the integration over the BZ was performed on a well converged Γ-centered $6 \times 6 \times 1$ k-point mesh, using the tetrahedron method with Blöchl corrections [25]. A structural relaxation in the system was performed via a quasi-Newton algorithm, using the exact Hellmann-Feynman forces acting on each atom. The total energies of the system were converged up to 1 meV/atom, while the residual force acting on each atom was less than 0.01 eV/Å.

To study the electronic and magnetic properties of the system, we simulated transition-metal monatomic chains on a Cu_3N/Cu(110) surface by means of a supercell approach. Our supercell structure contained a six-atomic layer slab of Cu(110) substrate with a $p(2 \times 3)$N-Cu(110) atomic arrangement of copper nitride surface layer repeated periodically and separated by a vacuum region of 8 Å. Such supercell employed for Cu_3N/Cu(110) contained also an infinite transition-metal chain placed on the bumping area of self-corrugated copper nitride and aligned along the [1-10] direction with a space separation of 10.8 Å between its images in the [001] direction (Fig. 1) [20]. This spacing is enough to avoid the spurious supercell effects in interchain interactions. For all calculations, the two bottom layers of the slab have been fixed under relaxation with an interlayer distance of 1.28 Å (which refers to the distance between the nearest crystalline planes along the
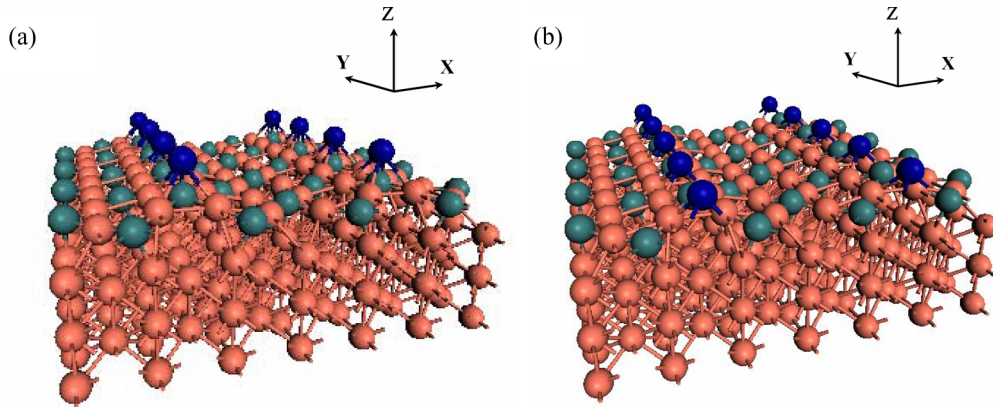
FIG. 1. Schematic view of the adsorbed $3d$ chains on the atop (a) and hollow (b) binding sites of the Cu$_3$N network. The actual relaxed atomic positions correspond to the case of the Co chain on Cu$_3$N. The blue (dark) spheres indicate the Co atoms, while the green (dark gray) and orange (light gray) spheres indicate N and Cu atoms, respectively.

[110] direction for Cu bulk), while other atomic layers were relaxed until the forces converged in the supercell.

Finally, we studied the time evolution of the magnetization under external magnetic field in supported monatomic magnetic chains via atomistic spin dynamics simulations. For this purpose we applied both a classical and a quantum Heisenberg model of Hamiltonian, as will be described in detail below.

III. RESULTS AND DISCUSSIONS

A. The structural properties and spin coupling in $3d$ chains

A combined high-resolution STM study and first-principles calculations, reported before [20], have shown that Cu and N atoms within the surface $p(2 \times 3)$ Cu$_3$N nitride phase are covalently polar bonded and yield a similar molecular network as reported for CuN$_2$ [7]. Owing to its intrinsic corrugation nature such a Cu$_3$N network serves as a perfect template for universal growth behavior of epitaxial atomic nanowires among a variety of $3d$, $4d$, and $5d$ elements. Nanowires made of these elements at the different coverages less than 0.50 ML occupy a single trough of a Cu$_3$N network and demonstrate an identical structure, uniform width ($\sim$1 nm), height ($\sim$0.12 nm), orientation ([1-10])and the same minimum separation. One can find more details in our previous paper [20]. Besides that, based on the structure information obtained by STM, the universal growth of linear nucleation clusters (linear chains) was revealed at the initial stage of epitaxy within the very lower coverages less than 0.01 ML. All of these linear chains are preferentially located at the bumping area within a trough of the $p(2 \times 3)$ Cu$_3$N network with random distribution and can serve as the nucleation centers of growth [26]. They can also display unique physical quantum properties. Consisting only of a few atomic spins, such atomic-scale structures are promising candidates for further technological implementations, for instance, in quantum computing or in high-density data-storage recording as feasible magnetic storage bits. To understand their binding properties and magnetic behavior, we simulate appropriately their atomic structure by deposition of infinitely long transition-metal (Mn, Fe, and Co) chains on top of the bumping area of the self-corrugated copper nitride surface plane. Based on the surface nitride

$p(2 \times 3)$ structure of the Cu$_3$N network, there are two available adsorption sites for considered $3d$ chains. In the first adsorption sites, the $3d$ chain atoms can be placed directly atop N atoms of the copper nitride surface plane [designated in Fig. 1(a) as "atop"], while in the second adsorption sites $3d$ atoms can sit in hollow sites laterally surrounded by four copper atoms of surface nitride (designated as "hollow"). When relaxing both adsorption geometries, the final relaxed atomic positions for deposited $3d$ chains are very similar. The difference between their heights (h) above the copper nitride is found to be at most $\Delta h^A \sim 0.05$ Å and $\Delta h^H \sim 0.21$ Å for the "atop" and "hollow" sites, respectively. The calculated adsorption energies (E^{ad}) indicate that $3d$ chain atoms have a high adhesion on the atop sites and energetically are more favorable than the hollow sites. Nevertheless, both sites are rather stable and in principle could be realized in experiment. Recently, for instance, an individual Mn and Fe atoms in dimer configurations have been arranged successfully directly on top of both N and Cu atoms on Cu$_2$N/Cu(100) in low-temperature STM experiments [6,11]. We observe also that adsorption of $3d$ adatoms atop Cu atoms of the Cu$_3$N network has a high adhesion, but causes a substantial displacement of copper underneath towards the underlying Cu(110) substrate. Finally, it breaks the bonds of Cu atoms with neighboring N atoms and makes them no longer be a part of the polar covalent network, while $3d$ adatoms almost take the place of dislodged Cu atoms. When relaxing adsorption geometry for atop site $3d$ chain atom and the nitrogen, sitting directly beneath, a rather distinct binding is revealed, which forms $3d$-N bonds of lengths lying in the range from 1.70 to 1.80 Å depending on d-band filling. There are also four subjacent Cu atoms of a surface plane which are next-nearest neighbors of the $3d$ ones at 2.76–2.87 Å distance from each chain atom. The distance between the $3d$ transition-metal atoms within the chain is 5.1 Å. This means that the direct interatomic interaction between the $3d$ chain atoms takes place across a "void" supplemented by a smaller indirect one intermediated by the substrate. The electronic density distribution analysis of the system shows that the $3d$ chain establishes the polar covalent bonds with nitrogen atoms lying below each chain atom and, hence, is covalently bonded with the Cu$_3$N network [see Fig. 2(a)]. For the relaxation in the hollow site we observe a significant
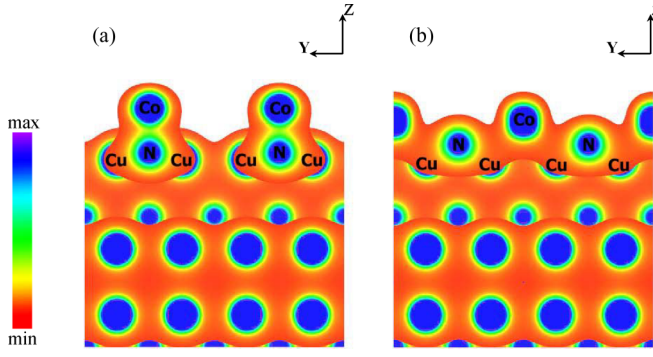
FIG. 2. The charge density distributions on a plane parallel to the Co chain adsorbed on the atop (a) and hollow (b) sites of the Cu₃N network.

vertical displacement of the lateral N atom between each pair of 3d chain atoms, relaxing outwards from the copper nitride surface plane towards the 3d chain. Finally after relaxation, the deposited transition-metal atom practically sits in between nearby nitrogen atoms and forms, together with nitrogen, a nearly linear diatomic chain. This situation is very similar to that reported before for the case of Cu₂N/Cu(100) [7]. The 3d-N bond length within diatomic chains is found around 2.75 Å with no relevant differences for the considered 3d chains. Besides there are four lateral Cu atoms of the underlying Cu₃N network at 2.44–2.56 Å distance from each 3d one. The calculations of density charge distribution show that 3d atoms in chains establish a covalent bonding with nitrogen, while the chains themselves bind metallically to the substrate through the copper atoms sitting below each chain one [see Fig. 2(b)]. Thus, there is a direct interatomic interaction between 3d atoms in chains through their neighboring nitrogen atoms and an indirect one through the substrate. Here, it is noteworthy that metallic type bonding with the substrate in the hollow site results in a weaker adhesion of the 3d chains than in the atop site with covalent type bonding. This is in agreement with previous results obtained for the case of 3d (Cr, Mn, Fe, Co) chains deposited on Cu₂N/Cu(100) substrate [19]. It was shown thereto the relationship between a type of chemical bonding to the substrate and magnetic intrachain interactions. Therefore, we next inquire into the magnetic properties of 3d chains placed on both adsorption sites of the Cu₃N network. Here, we consider only collinear

ferromagnetic (FM) and antiferromagnetic (AFM) intrachain spin configurations for each adsorption site, since we are mainly concerned with the general trends of magnetic behavior related to d-band filling and type of chemical bonding. For the magnetic ground-state configuration we present in Table I the results of spin-polarized calculations obtained for each deposited 3d chain. Among them, the total energy difference $\Delta E = E^{\mathrm{AFM}} - E^{\mathrm{FM}}$ between AFM and FM solutions, which allows us to estimate the strength of exchange coupling (J) of atomic spins. Assuming a Heisenberg model of interaction, one can obtain the value of exchange coupling for an infinite chain from a simple expression: $J = \frac{\Delta E}{4S^2}$, where S is the magnitude of an atomic spin. It is seen from Table I that the adsorption sites give rise to the distinct magnetic solutions with the same trends for the considered 3d chains. If a 3d chain sits in an atop site, it exhibits ferromagnetic coupling between spins of neighboring 3d atoms, while it exhibits antiferromagnetic coupling between them sitting in a hollow site. As expected, due to the stronger adhesion in the atop site, 3d atoms of chains have a stronger hybridization with a substrate and demonstrate smaller magnetic moments than in the hollow site. Moreover, the decrease of the magnetic moment from Mn to Co for both adsorption sites is a consequence of the 3d filling of the transition-metal minority bands. The results obtained for the order of magnitude and the sign of ΔE and J reveal that the transition metals interact magnetically along the chain through a completely different mechanism depending on the adsorption geometry. For the same interatomic distance and for a given d-band filling, the magnetic interaction along the chain can exhibit either ferromagnetic or antiferromagnetic coupling of atomic spins. The direct 3d-3d interaction along the chain deposited in the atop site determines the FM solution. However, in the hollow site this interaction is mediated by the interposing nitrogen atoms of the underlying Cu₃N network. In this case, as we demonstrated before, it is unlikely to have a direct overlapping between d orbitals of the chain 3d atoms. Their indirect 3d-3d interaction through the ligand 2p nitrogen orbitals exhibits a superexchangelike character, giving rise to a strong AFM solution. This kind of magnetic interaction has already been treated in detail for the case of finite Mn linear chains on a Cu₂N/Cu(100) substrate [14,15].

Now we turn to the discussion of the magnetic anisotropy energy (MAE) and the effect of electron correlations in deposited 3d chains. The values of single-site MAEs received within a plain DFT approach are shown in Table I. It is well

TABLE I. The calculated values of the energy difference (ΔE) between antiferromagnetic (AFM) and ferromagnetic (FM) states; their total (M) and orbital (M^L) magnetic moments directed along magnetization in x, y, and z axes; exchange couplings (J); magnetic anisotropy energy (MAE); and easy axis of magnetization for adsorbed 3d chains.

Adsorption site	Metall	$\Delta E = E^{\mathrm{AFM}}\text{-}E^{\mathrm{FM}}$ (meV)	M (μB)	M^L (μB)			J (meV)	MAE (meV/atom)	Easy axis
				m_x^L	m_y^L	m_z^L			
Atop	Mn	4.99	3.78	0.013	0.014	0.004	0.31	0.67	Y
	Fe	5.01	2.78	0.080	0.080	0.200	0.56	1.21	Z
	Co	15.22	1.67	0.210	0.226	0.357	3.80	2.30	Z
Hollow	Mn	− 52.55	4.27	0.018	0.013	0.012	− 3.28	0.12	X
	Fe	− 3.31	3.01	0.158	0.171	0.161	− 0.37	0.20	Y
	Co	− 6.32	1.89	0.280	0.306	0.251	− 1.58	0.93	Y

seen that at both adsorption sites there is a substantial increase of the MAE with d-band filling from Mn to the Co atom. For the Mn atom the easy axis of magnetization is along the chain direction (or Y axis) in the atop site, while it is along the in-plane direction (or X axis) in the hollow site. For the case of Fe and Co atoms the easy magnetization axis exhibits the same orientation, that is, along the out-of-plane direction (or Z axis) in the atop site, while it is along the chain direction (or Y axis) in the hollow site. Here it is worthy to note that a relatively small magnitude of MAE for Mn atom compared to the Fe and Co ones was revealed also in previous experimental and theoretical studies of individual $3d$ atoms placed on a $Cu_2N/Cu(100)$ substrate [7,12,13]. Besides that, our results demonstrate that the easy axis of magnetization, obtained for Fe and Co chain atoms in the hollow site, is directed across nearby nitrogen atoms, as was reported for individual Fe and Co atoms placed in between nitrogen atoms on a $Cu_2N/Cu(100)$ substrate. To bring insights into the origins of the MAE behavior, we analyze for the considered chains their electronic band structures. It has been shown clearly, through the second-order perturbative approach, that the density of states (DOS) in the vicinity of the Fermi level can be associated directly with the MAE [27,28]. In Fig. 3 we present, as an example, the total and orbital-resolved partial densities of states of an individual Co atom in a chain for both adsorption sites. As can be seen for both sites, the majority band (spin-up states) is fully occupied and thereby, ignoring the spin-flip terms between states, the predominant contribution to the magnetic anisotropy can be only attributed to the coupling between states in the minority band (spin-down states). Clearly, the visibly pronounced DOS peaks close to the Fermi level are mostly composed of the partial densities of states (PDOS) for minority d band, as shown in the insets of Fig. 3. After analyzing the spin-orbit coupling (SOC) between the different occupied and unoccupied eigenstates near the Fermi level, we find that in the case of the atop site the d_{xy}, d_{yz}, d_{xz}, and $d_{x^2-y^2}$ orbitals have the most dominant contributions to the magnetic anisotropy. Consistently, the SOC matrix elements obtained for these orbitals $\langle xy|\vec{L}|x^2-y^2\rangle$ and $\langle xz|\vec{L}|yz\rangle$ of the orbital moment operator ($\vec{L}$) provide the out-of-plane easy axes of magnetization for a Co chain. The same PDOS analysis applied for the hollow site reveals that in-plane magnetization direction obtained for the Co chain in this case is mostly determined by the SOC of the $d_{3z^2-r^2}$ orbital with the d_{xz} one, $\langle 3z^2-r^2|\vec{L}|xz\rangle$. However, there is a coupling between the d_{xy} and $d_{x^2-y^2}$ orbitals, $\langle xy|\vec{L}|x^2-y^2\rangle$, which contributes also to the MAE and favors the out-of-plane magnetization. Consequently, the interplay between these two couplings stated above determines the direction of the easy axes for the Co chain in the hollow site.

Further, we proceed in our study with Bruno's analysis, which allows us to understand the MAE behavior in terms of the variations of the orbital moments and, thus, related with orbital polarization below and above the Fermi level [29]. The direct link between the MAE (E_{ma}) and the orbital moment anisotropy (OMA) is read as $E_{ma} \approx \frac{\xi}{4}\Delta m^L$, where ξ is the spin-orbit constant of the magnetic chains and Δm^L is the orbital moment differences between two directions of magnetization. It means, in general, that the largest orbital moment component lies in the direction of the
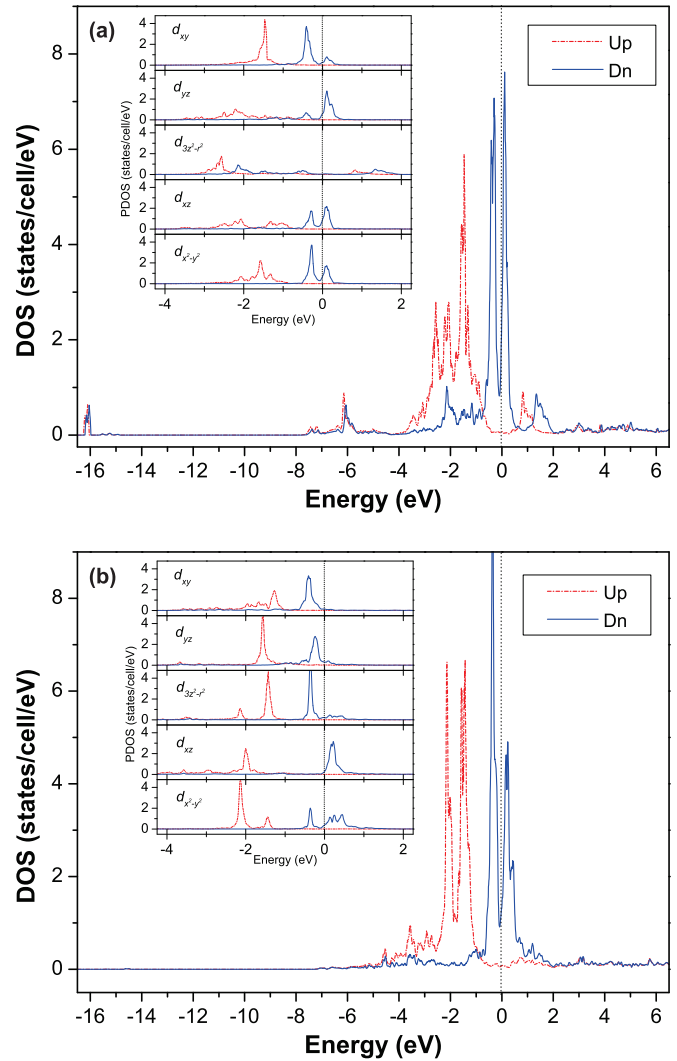

FIG. 3. Total densities of states (DOS) for Co atom in chain adsorbed on the atop (a) and hollow (b) sites of the Cu_3N network. The red (dashed-dotted) and blue (solid) curves represent the majority (spin-up) and minority (spin-down) states, respectively. The Fermi level is assigned by the vertical dotted line at zero energy. Insets: decomposed majority and minority d-orbital partial densities of state (PDOS) for Co atom on both adsorption sites.

easy magnetization axis. We calculate the orbital moments and present their m^L projection values on magnetization axes in Table I. One can observe that for all $3d$ chains Bruno's relation is valid and reproduces properly the sign and the trend of the calculated MAE.

B. Kinetic Monte Carlo (KMC) simulation of spins in $3d$ chains

Now we turn to the discussion of the evolution of the magnetization under external magnetic field (B) in magnetic $3d$ chains supported on a $CuN_3/Cu(110)$ surface via atomistic spin dynamics simulations. We present here our results for magnetization dynamics of ferromagnetically coupled Fe, Co, and Mn monatomic chains on a CuN_3 surface in the framework of the quasiclassical approach. As it was shown, the magnetic

atoms of these chains are placed on top of N, which are far enough apart (across a "void" of 5.0 Å), and demonstrating suitable values for exchange coupling and magnetic anisotropy energy. Further, we used them to fit, so far, an effective exchange coupling (J) and magnetic anisotropy constant (K) into a Hamiltonian of the classical Heisenberg model with an on-site uniaxial anisotropy and external magnetic field ($\vec{B}$) of the form

$$H = -\sum_{ij} J \vec{S}_i \vec{S}_j - \sum_i K (S_{z,i})^2 - \mu \sum_i \vec{S}_i \vec{B}, \quad (1)$$

where $\vec{S}_i$ is the normalized spin value at atomic site i and the summation ij is taken over all neighboring pairs of spins i and j. We investigate the spin dynamics of the system within the kinetic Monte Carlo method based on transition-state theory [30,31]. Such scheme was applied successfully to describe the ferromagnetic behavior (the shape of magnetization curves, coercivity, remanence, etc.) of monatomic Co spin chains on Pt surfaces [30,32]. In this scheme, the transition-state barrier, $\Delta E = (K + h_i)^2/4K$, where $h_i = (\sum_j J S_j + \mu B) S_i$ is the key parameter. The spin-flip rate is assumed to follow the Arrhenius law $\nu = \nu_0 \exp(-\Delta E_i/k_B T)$, where k_B is the Boltzmann constant and the prefactor ν_0 is assumed to be 10^9 Hz [30,31]. During simulations we have considered the temperature (T) of the deposited chains in the range up to 30 K, and their magnetization curves have been calculated. The external magnetic field was always applied along the easy axes of magnetization of the chains. At the lower temperatures the magnetization curves of deposited Fe, Co, and Mn monatomic chains exhibit hysteresislike behavior (ferromagnetic), which implies long-range ferromagnetic spin order, while at the higher temperature no hysteresis loop (paramagnetic) is observed at all. As an illustration, in Fig. 4 the magnetic response of the Co chain is presented for temperatures $T = 1.4$ K and $T = 11$ K. One can see that in the case of $T = 1.4$ K the magnetic signal is characterized by a hysteresis loop with a relatively large coercive field (H_C) about 3.3 T, while no magnetic signal is observed at higher temperature $T = 11$ K. Such variation of magnetic response can be ascribed by temperature-dependent coercivity [$H_C(T)$] determined from calculated hysteresis loops at different temperatures, as is presented in Fig. 4. By taking into account the thermal activation effect described by the Arrhenius law, the coercivity is expected to decrease exponentially with increasing temperature, $H_C(T) \sim (e^{T_B/T} - e)$, and vanishes at the blocking temperature (T_B). Above this temperature the system exhibits paramagnetic behavior. Fitting data points of coercivity, the corresponding value, $\sim$11 K, of blocking temperature for the Co chain was determined. It is close to the experimental value, $\sim$15 K, obtained for highly dense arrays of monatomic Co spin chains on vicinal Pt surface [33]. The same calculations applied for Fe and Mn chains revealed the blocking temperature less than $T_B < 2$ K, for both chains. It is clear why their temperature is so low, since their effective exchange coupling between atomic spins within chains is weaker in regard to the Co chain. Moreover, due to the larger value of magnetic anisotropy energy ($\sim$2.30 meV), we obtained the larger coercive field (up to 3.3 T) for a Co chain. Hence, we conclude that the strong exchange coupling
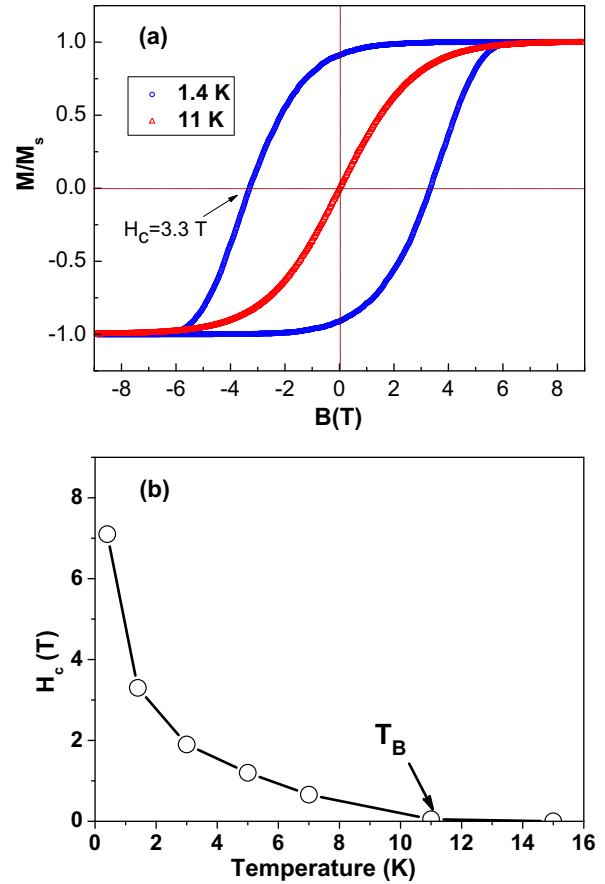

FIG. 4. Hysteresis loops for ferromagnetic Co chain deposited on the atop site of the Cu_3N template for representative temperatures $T = 1.4$ K (blue curve) and $T = 11$ K (red curve); (b) The temperature-dependent coercivity $H_C(T)$ determined from calculated M-B loops vanishes at the blocking temperature T_B. The magnetization M is normalized with respect to its saturation value M_s.

between atomic spins in chains is responsible for the onset of the magnetization curve, while the magnetic anisotropy determines the shape of this curve.

C. Quantum entanglement of spins in 3d chains

Further, we consider the spin dynamics in Fe, Co, and Mn chains in a $CuN_3/Cu(110)$ molecular network beyond the quasiclassical approach, where quantum effects can be very important at substantially low temperatures. For this purpose, we turn to the discussion of quantum entanglement in these chains, since this phenomenon can play an important role and be used as a potential resource for quantum information processing [34–36]. Two spins, S_1 and S_2, are entangled if the two-spin state can be, by no means, written as a product of single spin states. For mixed states the entanglement means the impossibility of decomposing the density matrix in term of separable states. A well known example of an entangled state is the singlet state of two spins, $[\frac{1}{\sqrt{2}} 1(|\uparrow\downarrow\rangle - |\downarrow\uparrow\rangle)]$ [34]. Measurement of one component of an entangled pair fixes the state of the other, implying nonlocal correlations.

Recent experiments evidenced that quantum entanglement can even exist in bulk systems [37,38] and can play a crucial role in macroscopic thermodynamical properties. There have also been many important experimental and theoretical studies related to quantum entanglement in spin systems [35,36,39–45]. Detection of entanglement can be made with the help of an entanglement witness (EW) [35,36]. Recently it has been shown that for complete separable states the average magnetic susceptibility of NS spins obeys the inequality [46]

$$\overline{\chi}(T) = \frac{\chi_x + \chi_y + \chi_z}{3} \geqslant \frac{(g\mu_B)^2 NS}{3k_B T}, \qquad (2)$$

where g is the Lande factor, μ_B the Bohr magneton, and T the temperature. The EW (W_e) is given by [46]

$$W_e = \frac{3k_B T \overline{\chi}(T)}{(g\mu_B)^2 NS} - 1. \qquad (3)$$

Systems presenting $W_e < 0$ are in an entangled state. The EW can be used to determine the temperature below which the spin entanglement exists. It should be noted that any EW is providing only a sufficient condition for the presence of entanglement. In the following, we focus on antiferromagnetic chains because an antiferromagnetic exchange between atoms in the chains allows the equilibrium density matrix to resemble the singlet ground state [45,47]; i.e., in the antiferromagnetic chains the ground state could be entangled in the absence of any external field. The entanglement vanishes above the temperature where the antiferromagnetic correlations vanish [45]. From the other side the ground state of ferromagnetic chains is a mixture of entangled and nonentangled states, and the EW cannot distinguish them [42]. It was demonstrated that the antiferromagnetic spin chains outperform the ferromagnetic spin chains as far as entanglement related properties are considered [48,49].

In particular, in even size chains a maximal entanglement is expected [50,51]. For calculations of the magnetic susceptibility in Eq. (2) we use the irreducible tensor operator technique [52] and the Heisenberg–Dirac–Van Vleck quantum spin Hamiltonian:

$$\hat{H} = -\sum_{ij} J \hat{S}_i \hat{S}_j - g\mu_B \sum_i \hat{S}_i \hat{B}, \qquad (4)$$

where $\hat{S}_i$ is the spin operator on the ith site and $\hat{B}$ is the magnetic field operator [53,54]. By means of this Hamiltonian, one can calculate the partition function of the system $Z = \mathrm{Tr}(e^{-\hat{H}/kT})$ and derive further the magnetic susceptibility $\bar{\chi} = (\frac{\partial M}{\partial B})_{H \to 0}$ from magnetization $M = NkT\frac{\partial \ln Z}{\partial B}$ [55]. We have calculated the EW for antiferromagnetic Mn, Fe, and Co chains of two to eight atoms. Our results presented in Fig. 5 reveal that the chains exhibit the quantum entanglement up to rather high temperatures. The largest entanglement temperature is found for Mn chains ($\sim$100 K).

Finally, we examine how the electron correlations can affect the quantum entanglement among the considered chains, due to the involved possible changes in electronic structure and orbital polarization of $3d$ chain atoms [15]. The obtained results demonstrate that the inclusion of the electron correlations does not change the EW essentially [56]. Thus, we believe that our calculations provide evidence of the existence
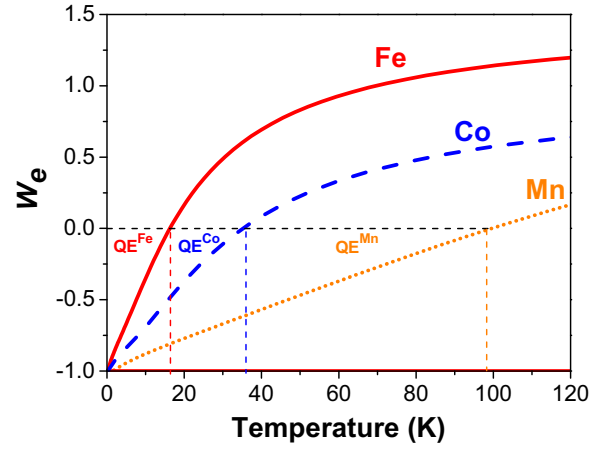

FIG. 5. Entanglement strength of Fe (red solid curve), Co (blue dashed curve), and Mn (yellow dotted curve) eight atomic chains deposited on a Cu_3N/Cu(110) substrate. QE denotes an entanglement area revealed for the considered $3d$ chain.

of quantum entanglement in the antiferromagnetic chains for realistic conditions.

IV. CONCLUSIONS

To sum up, in this work we have shown that a self-corrugated covalently bonded molecular Cu_3N network on a Cu(110) surface can serve as a good template to tailor magnetic interactions and dynamics of spins among transition-metal atoms by depositing $3d$ (Mn, Fe, and Co) chains on various adsorption sites. We find at these sites that, due to the different types of bonding on the decoupling copper nitride layer, the exchange interaction in atomic chains can lead to ferromagnetic or antiferromagnetic coupling of atomic spins along the chain. The spin dynamics simulations, based on classical and quantum approaches, demonstrate that the strength of the exchange interaction, over the value of the magnetic anisotropy energy, is the dominant character responsible for the onset of magnetization curves for ferromagnetic $3d$ chains and for possible existence of quantum entanglement in the antiferromagnetic ones for realistic conditions. We believe that our results are of major importance, since they clearly show a versatility of spin dynamics in supported nanostructures mediated by selecting suitable adsorption sites and magnetic interactions on a surface, which can open a ways for engineering of spins at the atomic scale in the future.

[1] J. V. Barth, G. Costantini, and K. Kern, Nature **437**, 671 (2005).

[2] P. Gambardella, S. Rusponi, M. Veronese, S. S. Dhesi, C. Grazioli, A. Dallmeyer, I. Cabria, R. Zeller, P. H. Dederichs, K. Kern, C. Carbone, and H. Brune, Science **300**, 1130 (2003); O. O. Brovko, P. A. Ignatiev, V. S. Stepanyuk, and P. Bruno, Phys. Rev. Lett. **101**, 036809 (2008).

[3] L. Zhou, J. Wiebe, S. Lounis, E. Vedmedenko, F. Meier, S. Blügel, P. H. Dederichs, and R. Wiesendanger, Nat. Phys. **6**, 187 (2010); A. A. Khajetoorians, J. Wiebe, B. Chilian, S. Lounis, S. Blügel, and R. Wiesendanger, *ibid.* **8**, 497 (2012).

[4] A. A. Khajetoorians, J. Wiebe, B. Chilian, and R. Wiesendanger, Science **332**, 1062 (2011).

[5] A. J. Heinrich, J. A. Gupta, C. P. Lutz, and D. M. Eigler, Science **306**, 466 (2004).

[6] C. F. Hirjibehedin, C. P. Lutz, and A. J. Heinrich, Science **312**, 1021 (2006).

[7] C. F. Hirjibehedin, C.-Y. Lin, A. F. Otte, M. Ternes, C. P. Lutz, B. Jones, and A. J. Heinrich, Science **317**, 1199 (2007).

[8] A. F. Otte, M. Ternes, K. Bergmann, S. Loth, H. Brune, C. P. Lutz, C. F. Hirjibehedin, and A. J. Heinrich, Nat. Phys. **4**, 847 (2008)

[9] A. F. Otte, M. Ternes, S. Loth, C. P. Lutz, C. F. Hirjibehedin, and A. J. Heinrich, Phys. Rev. Lett. **103**, 107203 (2009)

[10] S. Loth, S. Baumann, C. P. Lutz, D. M. Eigler, and A. J. Heinrich, Science **335**, 196 (2012).

[11] B. Bryant, A. Spinelli, J. J. T. Wagenaar, M. Gerrits, and A. F. Otte, Phys. Rev. Lett. **111**, 127203 (2013).

[12] A. B. Shick, F. Máca, and A. I. Lichtenstein, J. Appl. Phys. **105**, 07C309 (2009).

[13] A. B. Shick, F. Máca, and A. I. Lichtenstein, Phys. Rev B **79**, 172409 (2009).

[14] W. L. Scopel, P. Venezuela, and R. B. Muniz, Phys. Rev. B **79**, 132403 (2009).

[15] A. N. Rudenko, V. V. Mazurenko, V. I. Anisimov, and A. I. Lichtenstein, Phys. Rev B **79**, 144418 (2009).

[16] C.-Y. Lin and B. A. Jones, Phys. Rev B **83**, 014413 (2011).

[17] J. W. Nicklas, A. Wadehra, and J. W. Wilkins, J. Appl. Phys. **110**, 123915 (2011).

[18] R. Pushpa, J. Cruz, and B. Jones, Phys. Rev. B **84**, 075422 (2011).

[19] M. C. Urdaniz, M. A. Barral, and A. M. Llois, Phys. Rev. B **86**, 245416 (2012).

[20] X.-D. Ma, D. I. Bazhanov, O. Fruchart, F. Yildiz, T. Yokoyama, M. Przybylski, V. S. Stepanyuk, W. Hergert, and J. Kirschner, Phys. Rev. Lett. **102**, 205503 (2009).

[21] G. Kresse and J. Hafner, Phys. Rev. B **48**, 13115 (1993); G. Kresse and J. Furthmüller, Comput. Mater. Sci. **6**, 15 (1996).

[22] P. E. Blöchl, Phys. Rev. B **50**, 17953 (1994).

[23] J. P. Perdew, J. A. Chevary, S. H. Vosko, K. A. Jackson, M. R. Pederson, D. J. Singh, and C. Fiolhais, Phys. Rev. B **46**, 6671 (1992).

[24] H. J. Monkhorst and J. D. Pack, Phys. Rev. B **13**, 5188 (1976).

[25] P. E. Blöchl, O. Jepsen, and O. K. Andersen, Phys. Rev. B **49**, 16223 (1994).

[26] X.-D. Ma *et al.* (private communication).

[27] P. Ruiz-Diaz, T. R. Dasa, and V. S. Stepanyuk, Phys. Rev. Lett. **110**, 267203 (2013).

[28] D. S. Wang, R. Wu, and A. J. Freeman, Phys. Rev. B **47**, 14932 (1993).

[29] P. Bruno, Phys. Rev. B **39**, 865 (1989).

[30] Y. Li and B-G. Liu, Phys. Rev. B **73**, 174418 (2006).

[31] A. S. Smirnov, N. N. Negulyaev, W. Hergert, A. M. Saletsky, and V. S. Stepanyuk, New J. Phys. **11**, 063004 (2009).

[32] L. He, D. Kong, and C. Chen, J. Phys.: Condens. Matter **19**, 446207 (2007).

[33] P. Gambardella, A. Dallmeyer, K. Maiti, M. C. Malagoli, W. Eberhardt, K. Kern, and C. Carbone, Nature **416**, 301 (2002).

[34] M. A. Nielsen and I. L. Chuang, *Quantum Computation and Quantum Information* (Cambridge University Press, Cambridge, UK, 2000).

[35] R. Horodecki, M. Horodecki, and K. Horodecki, Rev. Mod. Phys. **81**, 865 (2009).

[36] L. Amico, A. Osterloh, and V. Vedral, Rev. Mod. Phys. **80**, 517 (2008).

[37] S. Ghosh, T. F. Rosenbaum, G. Aeppli, and S. N. Coopersmith, Nature **425**, 48 (2003).

[38] C. Brukner, V. Vedral, and A. Zeilinger, Phys. Rev. A **73**, 012110 (2006).

[39] A. Candini, G. Lorusso, F. Troiani, A. Ghirri, S. Carretta, P. Santini, G. Amoretti, C. Muryn, F. Tuna, G. Timco, E. J. L. McInnes, R. E. P. Winpenny, W. Wernsdorfer, and M. Affronte, Phys. Rev. Lett. **104**, 037203 (2010).

[40] G. A. Timco, S. Carretta, F. Troiani, F. Tuna, R. J. Pritchard, C. A. Muryn, E. J. L. McInnes, A. Ghirri, A. Candini, P. Santini, G. Amoretti, M. Affronte, and R. E. P. Winpenny, Nat. Nanotechnol. **4**, 173 (2009).

[41] M. S. Reis, S. Soriano, A. M. dos Santos, B. C. Sales, D. O. Soares-Pinto, and P. Brandão, Europhys. Lett. **100**, 50001 (2012).

[42] D. O. Soares-Pinto, A. M. Souza, R. S. Sarthour, I. S. Oliveira, M. S. Reis, P. Brandão, J. Rocha, and A. M. dos Santos, Europhys. Lett. **87**, 40008 (2009).

[43] A. M. Souza, M. S. Reis, D. O. Soares-Pinto, I. S. Oliveira, and R. S. Sarthour, Phys. Rev. B **77**, 104402 (2008).

[44] I. Bose and A. Tribedi, Phys. Rev. A **72**, 022314 (2005).

[45] D. Das, H. Singh, T. Chakraborty, R. Krishna Gopal, and C. Mitra, New J. Phys. **15**, 013047 (2013).

[46] M. Wiesniak, V. Vedral, and C. Brukner, New J. Phys. **7**, 258 (2005).

[47] F. Troiani and M. Affronte, Chem. Soc. Rev. **40**, 3119 (2011).

[48] S. Sarkar, J. Quant. Inf. Sci. **1**, 105 (2011).

[49] A. Bagat and S. Bose, Adv. Math. Phys. **2010**, 127182 (2010).

[50] S. Oh, M. Friesen, and X. Hu, Phys. Rev. B **82**, 140403(R) (2010).

[51] S. Holzberger, T. Schuh, S. Blugel, S. Lounis, and W. Wulfhekel, Phys. Rev. Lett. **110**, 157206 (2013).

[52] J. J. Borras-Almenar, J. M. Clemente-Juan, E. Coronado, and B. S. Tsukerblat, Inorg. Chem. **38**, 6081 (1999); J. Comput. Chem. **22**, 985 (2001); MAGPACK code was used.

[53] Note that the Heisenberg term commutes with the Zeeman one. It allows as to use the magnetic susceptibility for calculations of the *EW*; see also Refs. [41,43,44]. The effect of the magnetic anisotropy on the magnetic susceptibility of studied chains is rather small.

[54] M. S. Reis, Comput. Phys. Commun. **182**, 1169 (2011).

[55] O. O. Brovko, O. V. Farberovich, and V. S. Stepanyuk, J. Phys.: Condens. Matter **26**, 315010 (2014).

[56] We have applied for d orbitals effective on-site Coulomb interactions $U_{\text{eff}} = U - J_H$ in the framework of the DFT+U approach and repeat our study of magnetic interactions within $3d$ chains using conventional values of $U_{\text{eff}} = 5.0$, 1.1, and 0.8 eV for Mn, Fe, and Co, respectively. The obtained results for an atomic spin (S), the energy difference (ΔE), and exchange coupling (J), demonstrate a limited effect of U_{eff} on magnetic interactions among all considered chains. We find that the DFT+U approach decreases the strength of exchange coupling between chain $3d$ atoms, but does not change the general trends in the entanglement strength obtained within a DFT one.